

# Experimental and model-based analysis of combustion and auto-ignition of gasoline and three surrogate fuels in a single-cylinder research engine operated under knocking conditions

International J of Engine Research  
2023, Vol. 24(6) 2727–2738  
© IMechE 2022  
Article reuse guidelines:  
sagepub.com/journals-permissions  
DOI: 10.1177/14680874221133143  
journals.sagepub.com/home/jer  


Magnus Kircher<sup>1</sup> , Jonathan Schneider<sup>2</sup>, Sebastian Popp<sup>1</sup>,  
Sandro Gierth<sup>1</sup>, Marco Günther<sup>2</sup> and Christian Hasse<sup>1</sup> 

## Abstract

A systematic analysis of knocking combustion at the knock limit in a single-cylinder research engine is conducted. Both experimental and numerical methods are used to investigate the physical phenomena involved in knocking combustion. While real gasoline fuel can be used directly in experimental studies, this is not feasible in numerical simulations. Here, surrogate fuels with a reduced number of components defined to match the desired properties, such as knock resistance, are employed. In this work, standard gasoline and three surrogate fuels are considered. Differences in composition complexity are covered by selecting isooctane and two toluene reference fuels (TRF) with ethanol addition, all of which exhibit negative temperature coefficient (NTC) behavior in which auto-ignition delay times increase with increasing temperature. Spark timing sweeps at two engine speeds show that the knock resistance of the fuels correlates with the respective research octane number (RON). Isooctane is found to have higher knock resistance and higher sensitivity to engine speed than standard gasoline. One of the two TRFs studied shows good agreement with gasoline in terms of combustion and knock characteristics. The lower knock resistance of the other TRF indicates a non-linear dependence between mixture composition and knock resistance. A strong relative increase in knock resistance at higher engine speeds suggests a possible influence of NTC behavior at lower engine speeds. In the subsequent model-based analysis, the fuel influence on combustion and auto-ignition is investigated, and the laminar burning velocities are found to correlate well with the observed heat durations. While auto-ignition may be triggered by a cool spot at the lower engine speed and at operating conditions within the NTC regime, auto-ignition at the higher engine speed is assumed to be initiated by hot spots. These different mechanisms for initiating auto-ignition were identified as a potential explanation for the different knock resistances observed.

## Keywords

SI engine, auto-ignition, knock, surrogate fuels, NTC

Date received: 19 July 2022; accepted: 22 September 2022

## Introduction

Downsizing is a promising way of increasing the efficiency of internal combustion engines.<sup>1</sup> However, the associated higher cylinder pressures favor knocking combustion. This sets a limit on efficiency due to potential engine damage. The relevance of knocking combustion is summarized in a recently published article by Wang et al.<sup>2</sup> In the past, various theories of knocking combustion have been proposed to explain its occurrence by either auto-ignition, detonation, or a combination of

<sup>1</sup>Department of Mechanical Engineering, Simulation of reactive Thermo-Fluid Systems, Technical University of Darmstadt, Darmstadt, Germany

<sup>2</sup>Chair of Thermodynamics of Mobile Energy Conversion Systems, RWTH Aachen University, Aachen, Germany

### Corresponding author:

Magnus Kircher, Technical University of Darmstadt, Department of Mechanical Engineering, Simulation of Reactive Thermo-Fluid Systems, Otto-Berndt-Straße 2, Darmstadt 64287, Germany.  
Email: kircher@stfs.tu-darmstadt.de

both.<sup>3–5</sup> This work focuses on the knock limit, where the knock intensity is low and can be controlled by adjusting the spark timing. Knock is assumed to be initiated by auto-ignition events in the unburned mixture ahead of the regular flame front, as first observed by Spicher et al.<sup>6</sup> Several studies have shown that different propagation modes can develop after an initial hot spot triggered auto-ignition event.<sup>7–9</sup>

In the past, both experimental and numerical methods have contributed to the understanding of the phenomena leading to knocking combustion. For experimental investigations of knocking combustion, the usage of conventional gasoline fuels is the obvious choice (e.g. for the engine measurements performed in studies by Robert et al.<sup>10</sup> and Fontanesi et al.<sup>11</sup>). These consist of many different hydrocarbons, such as alkanes and aromatics. However, the evaluation of the knock resistance is based on Primary Reference Fuels (PRFs). By adjusting the relative proportion of heptane and isooctane in these blends, the research octane number (RON) and the motor octane number (MON) are determined. The octane sensitivity (OS) is defined as the difference between RON and MON, and has positive values for real gasoline fuels.<sup>12</sup>

In the absence of information or standardization of the exact composition of gasoline, numerical studies usually use surrogate fuels consisting of a reduced number of known components.<sup>12</sup> Especially for knock investigations, it is necessary that burning velocity and auto-ignition delay times are properly captured by the surrogate formulation. In several recent numerical studies, isooctane has been used as a surrogate fuel to investigate knocking combustion.<sup>13–15</sup> However, the RON and MON of isooctane are identical by definition, which leads to an unrealistic OS of zero.

Lacour and Pera<sup>16</sup> showed that by defining three-component mixtures of isooctane, heptane and toluene, suitable surrogate fuels for gasoline can be defined. These Toluene Reference Fuels (TRFs) mimic the aromatic content of real gasoline fuels and can provide a good match for gasoline fuel target properties such as RON, MON, OS, liquid density and H/C ratio.<sup>17</sup> The above-mentioned studies by Robert et al.<sup>10</sup> and Fontanesi et al.<sup>11</sup> incorporated TRFs for the numerical investigations. To take into account the alcohol content of modern gasoline fuels, ethanol is added to TRFs.<sup>18</sup>

The increasing complexity of surrogate fuels allows capturing important aspects of long-chained hydrocarbons, such as those present in gasoline. Low-temperature chemistry can often be observed for these, leading to a more complex auto-ignition behavior. As a result, many large hydrocarbons exhibit negative temperature coefficient (NTC) behavior.<sup>19–21</sup> While typically the auto-ignition delay time decreases with increasing temperature, inside the NTC regime, the auto-ignition delay times increase with rising temperature (cf. Figure 1). The relevance of NTC for knocking combustion was investigated in several studies, which have found that low NTC sensitivity fuels show high OS.<sup>18,22,23</sup>

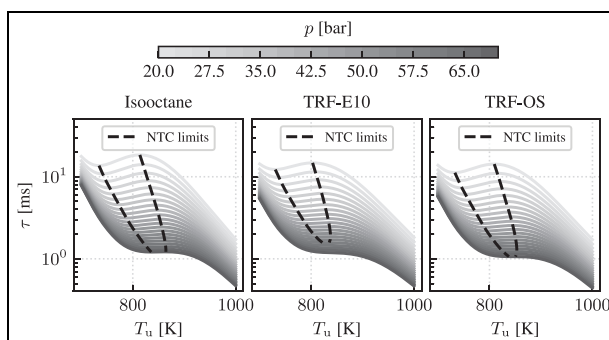


**Figure 1.** Influence of unburned temperature  $T_u$  and pressure  $p$  on auto-ignition delay times of stoichiometric mixtures. Isooctane shown on the left side, TRF-E10 in the middle and TRF-OS on the right side. The NTC limits are depicted as dashed lines.

For a fuel with NTC behavior, Dai et al. showed in a numerical study that after auto-ignition triggered by a cool spot, propagation modes similar to hot-spot auto-ignition could develop, and concluded that this could lead to knocking combustion.<sup>24</sup> To the authors' knowledge, there is no systematic study investigating such behavior in a combined experimental and numerical analysis.

The objective of this work is to systematically investigate the knocking behavior of standard gasoline fuel and three surrogate fuels of different complexity, which show NTC behavior. Isooctane and two TRFs with different compositions leading to different values for the OS are investigated as surrogate fuels. In an experimental study, spark timing sweeps are conducted to investigate the differences in knocking behavior of the fuels. These investigations are performed for different engine speeds. The experimental findings are complemented by a model-based analysis of the surrogate fuels. The fuel influence on combustion and auto-ignition is investigated. Special focus is given to the NTC behavior and its potential influence on auto-ignition under knocking conditions.

The remainder of the paper is structured as follows. First, the experimental setup as well as the fuels investigated are presented. Then, the data processing is described and the main experimental results are discussed. This is followed by the discussion of the model-based analysis. The paper concludes with a summary of the key findings.

## Fuel selection

Knocking combustion is experimentally investigated for research grade RON95E10 gasoline as the reference fuel, as well as three surrogate fuels. The selection of surrogate fuels captures a variation in compositional complexity as well as expected knock resistance. The suitability as a reference surrogate fuel for knock investigations can be determined in comparison with

**Table 1.** Characteristic parameters and composition of the fuels under investigation.

Parameter	RON95E10	Isooctane	TRF-E10	TRF-OS
RON/-	96.4	100	96.6	95.3
MON/-	86.3	100	88.3	92.6
OS/-	10.1	0	8.3	2.7
H/C/-	1.87	2.25	1.93	2.07
$\rho/\text{kg}/\text{m}^3$	739.9	690	739.6	714.6
Ethanol/mass-%	—	—	9.8	5.3
Toluene/mass-%	—	—	30.3	17.4
Heptane/mass-%	—	—	13.4	11.3
Isooctane/ mass-%	—	100	46.3	66

RON95E10. The characteristic parameters of the fuels are listed in Table 1.

The first surrogate fuel selected is isooctane, a commonly used single-component surrogate fuel for knock investigations. With a RON and MON of 100 by definition, isooctane is expected to show a higher knock resistance than the reference RON95E10.

In addition, two TRFs are investigated in this study. The first TRF, TRF-E10, is based on an experimental and numerical study.<sup>25</sup> The composition has been optimized to match well with RON95E10 in terms of RON, MON, H/C and aromatic content. The auto-ignition delay times were found to be consistent with RON95E10 measurements.<sup>25</sup> Therefore, TRF-E10 is expected to have a similar knock behavior as the reference RON95E10.

The second TRF, TRF-OS, is chosen to investigate the influence of octane sensitivity (OS), which is related to the change in reactivity with pressure and temperature.<sup>2</sup> TRF-OS is based on a study by Kim et al.,<sup>18</sup> in which the two-stage auto-ignition behavior and OS of four-component TRFs were investigated. Previous studies have found that fuels with similar RON, but higher OS, show higher knock resistance.<sup>26–28</sup> With a similar RON to RON95E10 but a significantly lower OS, TRF-OS is expected to show lower knock resistance in comparison.

### Auto-ignition delay times

The surrogate fuels are further characterized by analysis of the auto-ignition delay times based on 0-D homogeneous reactor calculations performed with an in-house solver.<sup>29</sup> A detailed mechanism developed for the TRF-E10, which considers 485 species and 2081 reactions,<sup>25</sup> is used to perform the calculations for all surrogate fuels at stoichiometric mixture. The sensitivity of the auto-ignition delay times to the unburned temperatures  $T_u$  and the pressures  $p$  is depicted in Figure 1. Isooctane is shown on the left side, TRF-E10 in the middle and TRF-OS on the right side. All three surrogate fuels show a distinctive NTC regime for the thermodynamic conditions investigated, with the auto-ignition delay times increasing between approximately

**Table 2.** Engine geometry and operating conditions.

Parameter	Value
Stroke	90.5 mm
Bore	75 mm
Compression ratio	11.83:1
Number of valves	2/2
Max valve lift	8 mm
Valve angle	22.5°
Valve diameter (In/Ex)	32/26 mm
Intake air pressure	ambient
Exhaust air pressure	ambient
Ambient air pressure	1013 mbar
Oil and coolant temp.	90°C

750 K and 850 K. The respective limits of the NTC regime are highlighted by dashed lines. The NTC limits of isooctane and TRF-OS show a similar range. For TRF-E10, the NTC regime narrows considerably with increasing pressure and finally disappears at the highest pressures investigated. Isooctane and TRF-OS show higher pressure sensitivity than TRF-E10, resulting in a wider range of auto-ignition delay times in the NTC range. In summary, the differences observed here are nevertheless not very pronounced.

### Experimental setup

The knocking behavior of the four different fuels is investigated in a single-cylinder research engine (SCRE) under stoichiometric operating conditions. To ensure a homogeneous mixture inside the cylinder, port-fuel injection (PFI) is used in this study. This avoids possible interference caused by direct injection, for example, mixture inhomogeneities or local temperature differences due to different latent heats of vaporization. The engine geometry and operating conditions are listed in Table 2. More details on the engine can be found in previous studies.<sup>30–32</sup>

### Measurement setup

The pressure in the cylinder is measured with two flush-mounted KistlerA6061B piezoelectric pressure transducers opposite each other in the combustion chamber roof between the intake and exhaust valves. Two transducers are used for redundancy. The pressure values given in this work always refer to the average of both pressure transducers. The pressures in the intake and exhaust manifolds are measured with Kistler 4045-A5 piezoresistive pressure transducers. The position of the crank shaft is measured with an optical encoder with a 0.1 °CA resolution. The measurement signals are processed via Kistler 5064 charge amplifiers and an FEV combustion analysis system (FEVIS). Coolant and oil temperatures are conditioned to 90°C. The engine is coupled to an eddy-current brake and an electric dynamometer to maintain the desired engine speed

**Table 3.** Operating point definition.

Parameter	OP1500	OP2500
Engine speed/r/min	1500	2500
IMEP/bar		10
IVO/°CA aTDC		15
EVC/°CA aTDC		-26
Spark timing		var.

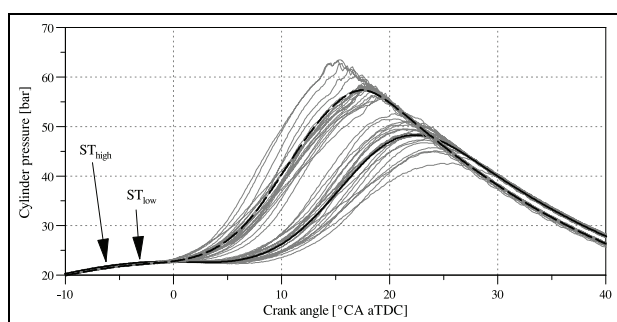


**Figure 2.** Mean pressure traces for two spark timings ( $ST_{low} = -3^{\circ}\text{CA aTDC}$ , shown as solid line and  $ST_{high} = -6.5^{\circ}\text{CA aTDC}$ , shown as dashed line) as well as 20 single cycle pressure traces each.

with an accuracy of  $\pm 1$  r/min, regardless of the engine load. The intake air mass flow is measured via a hot-film air mass meter. The relative air/fuel ratio of the exhaust gas is derived according to Spindt<sup>33</sup> with the extension for oxygenated fuels by Bresenham et al.<sup>34</sup> Static pressures and all temperatures are averaged over a 30-s time period.

### Operating points

In this work, two reference operating points (OPs), OP1500 and OP2500, are defined with different engine speeds. These engine OPs are chosen to investigate the knock onset and the influence of engine speed for all four fuels under similar boundary conditions, and are listed in Table 3. To minimize valve overlap and internal exhaust gas recirculation (EGR), identical valve timings of intake valve opening (IVO) 15 °CA aTDC and exhaust valve closing (EVC) 26 °CA bTDC at 1 mm lift are chosen for both OPs.

### Measurement procedure

To investigate the combustion behavior at the onset of knock, spark timing sweeps are conducted to vary the combustion phasing in terms of 50% fuel mass fraction burned (MFB50).

Starting from a spark timing well below the knock limit, the spark timing is incrementally advanced, which shifts the center of combustion (MFB50) forward and increases cylinder pressure and maximum

temperature. Therefore, the likelihood of auto-ignition increases. As an example, two spark timings at OP1500 ( $ST_{low} = -3^{\circ}\text{CA aTDC}$  and  $ST_{high} = -6.5^{\circ}\text{CA aTDC}$ ) are shown in Figure 2. For each spark timing, 20 exemplary single cycle pressure traces are plotted, as well as the resulting mean pressure trace.

For  $ST_{low}$ , only a few knocking cycles with low amplitude of the pressure oscillation are recorded. At  $ST_{high}$  the mean peak pressure position is advanced, the peak pressure is higher and almost all cycles show significant pressure oscillations. Due to possible engine damage, the increasing pressure oscillations set a limit to the spark advance. For the different spark timings, the engine load is kept constant by adjusting the intake manifold pressure. Due to the characteristic cycle-to-cycle variations (CCV) in each operating condition, suitable auto-ignition conditions are not reached for every cycle, but rather only for the fastest burning cycles with the highest cylinder pressures and temperatures. Therefore, the knock-relevant quantities, discussed in the next section, are retrieved by averaging over the 1000 recorded cycles in each operating condition. In order to compare the knock behavior of the fuels investigated in this study (cf. Table 1), different spark timings are chosen for each fuel to achieve similar knock intensity levels. This in turn leads to different thermodynamic conditions, which have to be considered when interpreting the results.

### Experimentally obtained knock quantities

The following quantities are obtained from 1000 individual cycles per parameter variation and discussed in the next section.

**Knock intensity.** The high-resolution pressure trace is used to characterize knock intensity. First, the high-frequency part of the pressure trace is separated from the low-frequency part by a weighted moving average low-pass filter. The low-frequency component corresponds to the mean pressure trace in the cylinder, and the high-frequency component contains the pressure oscillations induced by auto-ignition. Subsequently, from the filtered high-frequency component of the cylinder pressure  $p$ , which is calculated by subtracting the low-pass filtered signal from the unfiltered signal, the characteristic value Knock-Peak-Peak (KPP) can be determined, as depicted in Figure 3. Based on all cycles in one operating condition, the average value  $KPP_{mean}$  can be calculated.

**Variation of knock intensity.** The standard deviation of KPP ( $\sigma_{KPP}$ ) is calculated from the variance of the cycle-individual KPP values in each operating condition. Therefore, it can be used as a parameter describing the cyclic variations in knock intensity.

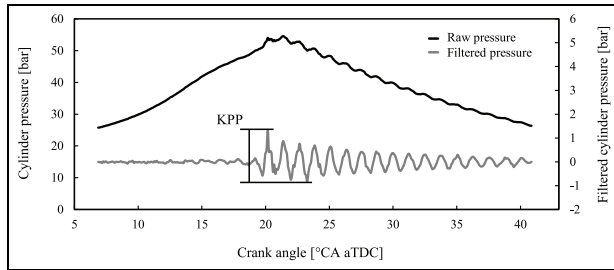


**Figure 3.** Example of a single cycle raw pressure trace with the corresponding filtered pressure trace and the parameter KPP.

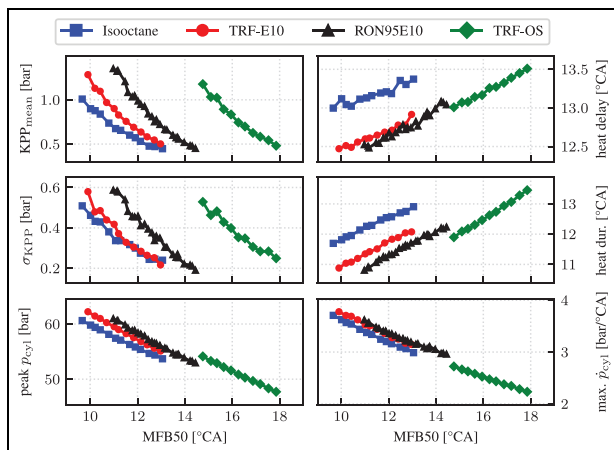


**Figure 4.** Overview of the experimental knock quantities for the four fuels under investigation at OP1500 (cf. Table 3).

**Heat delay & heat duration.** To calculate the heat release rate, the high-resolution pressure trace is further analyzed in a detailed offline model based on the Rassweiler and Withrow method<sup>35</sup> using the FEVIS system. The polytropic coefficients of compression and expansion are fitted to the individual pressure traces of the combustion cycles. This enables the calculation of the MFB from the pressure data, providing key parameters such as the crank angle at MFB50, the heat delay, calculated from spark timing (ST) to MFB10, and the heat duration, calculated from MFB10 to MFB90.

**Peak pressure & pressure rise.** Since cylinder pressure is a key factor influencing auto-ignition, the average maximum cylinder pressure and the maximum rate of pressure rise are calculated from the pressure transducer signal.

## Experimental results

In the following, the previously introduced experimental knock quantities are discussed for the two operating points investigated (cf. Table 3).

## Analysis of OP1500

The measurement results for OP1500 are shown in Figure 4. The baseline RON95E10 shows low  $KPP_{\text{mean}} = 0.47$  bar at  $MFB50 = 14.3^\circ\text{CA}$ , increasing with earlier spark timing to a maximum  $KPP_{\text{mean}} = 1.35$  bar at  $MFB50 = 11.0^\circ\text{CA}$ . The increase in knock intensity toward earlier MFB50 is exponential. With earlier MFB50, heat delay and heat duration decrease linearly, while pressure rise rate and peak cylinder pressure increase up to  $p_{\text{cyl}} = 60.9$  bar at  $MFB50 = 11.0^\circ\text{CA}$ . The standard deviation of  $KPP_{\text{mean}}$ ,  $\sigma_{KPP}$ , increases exponentially with earlier MFB50, similar to  $KPP_{\text{mean}}$ , indicating increased CCV with earlier spark timings. In general, it is found that as MFB50 decreases, the combustion process becomes shorter and higher pressures and mean knock intensities occur, as well as higher cyclic variations. This is observed for all tested fuels.

Regarding surrogate fuels, isooctane, as the single-component fuel, is discussed first. With a RON of 100 by definition, significant knock intensities occur only at very early spark timings and hence MFB50 with high cylinder pressures and rates of pressure rise. Thus, isooctane exhibits a high knock resistance, as expected. The combustion behavior of isooctane differs slightly from that of the baseline RON95E10. The calculated heat delay and heat duration at comparable MFB50 are higher for isooctane because the cylinder pressure generally increases less. To achieve the same MFB50, isooctane needs to be ignited earlier. The lower cylinder pressures corresponds to a relatively slow heat release rate of isooctane. Due to these differences in combustion characteristics and the significantly higher knock resistance, isooctane can only be used to a limited extent as a surrogate fuel for knock investigations if comparison is to be made with RON95E10.

TRF-E10 closely matches RON95E10 in terms of heat delay and heat duration, as well as peak pressure and pressure rise rate. For TRF-E10 comparable KPP values at only slightly earlier MFB50 ( $\Delta^\circ\text{CA} < 1.5^\circ$ ) compared to RON95E10 are observed. The similar behavior in terms of knock onset and increase in KPP with ignition timing demonstrates that it is suitable as a surrogate fuel.

As expected, TRF-OS with the lowest RON is the least knock resistant fuel. Comparable KPP values to those of RON95E10 are observed already at late MFB50 and therefore low peak cylinder pressures. However, reaching similar knock intensities at much less critical conditions is unexpected for TRF-OS given its individual composition. With a significantly higher content of isooctane and lower content of toluene, heptane and ethanol compared to TRF-E10, one would expect its knock behavior to be closer to that of isooctane. This suggests a strong non-linear dependence between the composition of the TRF and the knock resistance. Considering heat delay and heat duration, TRF-OS closely matches the values of isooctane,

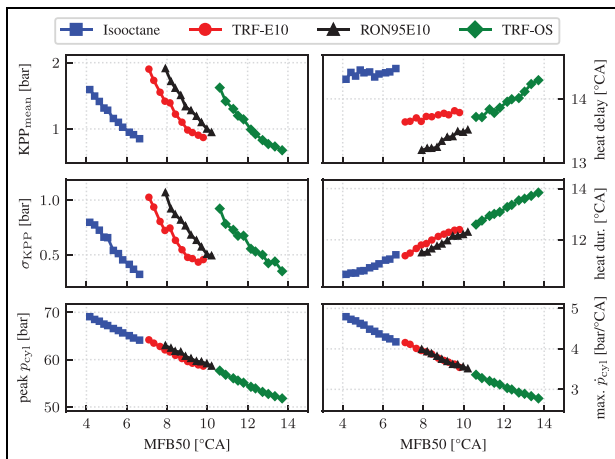


**Figure 5.** Overview of the experimental knock quantities for the four fuels under investigation at OP2500 (cf. Table 3).

although at later MFB50, providing no further insight into this outlier behavior. Since the different thermodynamic conditions compared to the other fuels at identical knock intensity or MFB50 make further experimental analysis of TRF-OS difficult, analyses beyond the experimental investigations are required. Therefore, a model-based analysis of the experimental results is performed and discussed after the results for OP2500 (Section Model-based analysis of experimental results). Here, special emphasis is put into the analysis of NTC relevance for the operating conditions investigated, as previous experimental studies have shown a correlation of low OS with strong NTC behavior.<sup>22,23,36</sup>

The standard deviation of KPP is directly proportional to the average KPP for all four fuels. With identical MFB50, eliminating the influence of combustion phasing on CCV in comparison, a significant influence of the fuel on  $\sigma_{KPP}$  similar to that on KPP is observed. Since TRF-OS reaches potentially destructive KPP values before reaching MFB50 values similar to those of the other fuels, a direct comparison is not possible here. However, since TRF-OS reaches the same levels of cyclic variability of knock intensity at later spark timings and therefore less critical conditions, the outlier behavior of TRF-OS becomes apparent. The peak cylinder pressure is shown to be fuel dependent both at identical combustion phasing, where it is lowest for isooctane and highest for TRF-E10, and at identical  $KPP_{mean}$ , where it is highest for isooctane and lowest for TRF-OS. This again corresponds well with the order of knock resistance according to RON. The maximum rate of pressure rise appears to be less dependent on fuel composition than on MFB50.

### Analysis of OP2500

The measurement results for OP2500 are shown in Figure 5. The increased engine speed leads to higher flow velocities and reduced residence times. Relevant knock intensities only occur at earlier spark timings

compared to those discussed for OP1500. As a result, for RON95E10, the MFB50 at which the mean knock intensity  $KPP_{mean} = 1$  bar is reached shifts by 2 °CA forward from  $MFB50 = 12.0^{\circ}CA$  at  $n_{engine} = 1500$  r/min to  $MFB50 = 10.0^{\circ}CA$  at  $n_{engine} = 2500$  r/min. The magnitude of this shift in MFB50 can be considered as a relative increase in knock resistance as a function of engine speed and is similar for TRF-E10 (1.7 °CA), but significantly higher for TRF-OS (3 °CA) and isooctane (3.7 °CA).

While the heat delay and heat duration for RON95E10, TRF-OS and TRF-E10 generally increase with higher engine speed, the heat delay of isooctane increases but the heat duration decreases significantly. The longer heat delay is attributed to increased knock resistance. The lower heat duration indicates a faster combustion and thus faster consumption of the end-gas volume which reduces the time available for the development of a potential auto-ignition. The strong relative increase in knock resistance of TRF-OS results in knock behavior more similar to that of RON95E10 and TRF-E10 at OP2500. This also suggests an NTC influence in OP1500, which will be investigated in the model-based analysis.

Similar to OP1500, TRF-E10 generally exhibits knock and combustion behavior very similar to RON95E10. They closely match in terms of heat duration, although combustion starts somewhat slower for TRF-E10, as indicated by the higher heat delay.

In summary, the experimental data show good agreement between the TRF-E10 surrogate and the baseline RON95E10 for most relevant parameters at both engine speeds. As expected, the order of fuels in terms of knock resistance correlates with their respective RON at both operating points. Isooctane reaches the earliest MFB50 at comparable mean knock intensities due to its high knock resistance, which strongly increases with engine speed. Considering its composition, TRF-OS shows an unexpectedly low knock resistance for OP1500, increasing, however, for OP2500. As this is attributed to potential NTC influence, investigation of the NTC behavior of the fuels as a potential source of the different knock limits of the surrogate fuels is a particular aspect of the subsequently conducted model-based analysis.

### Model-based analysis of experimental results

For the model-based analysis, a reduced number of operating points of the experimental database (cf. Figures 4 and 5) is chosen. For every surrogate fuel, a late (LST), an intermediate (IST), and an early spark timing (EST) are investigated to cover the ranges of MFB50 and knock intensity. The selection aims for similar knock intensities of the fuels for the respective spark timings and is summarized in Table 4.

**Table 4.** Summary of operating points investigated in the model-based analysis.

Fuel	Alias	OPI500		OP2500	
		MFB50	KPP <sub>mean</sub>	MFB50	KPP <sub>mean</sub>
Isooctane	LST	13.0	0.45	6.6	0.85
	IST	11.6	0.60	5.3	1.16
	EST	9.6	1.01	4.1	1.60
TRF-E10	LST	13.0	0.50	9.5	0.87
	IST	11.5	0.76	8.4	1.22
	EST	9.9	1.28	7.0	1.90
TRF-OS	LST	17.8	0.45	12.3	0.92
	IST	16.2	0.73	10.9	1.41
	EST	14.7	1.01	10.6	1.62

From a modeling perspective, knocking combustion is characterized by the two competing processes of flame propagation and auto-ignition. By relating these to important fuel properties, namely the laminar burning velocity  $s_L$  of the mixture and the auto-ignition delay time  $\tau$ , the influence of fuel chemistry can be investigated.

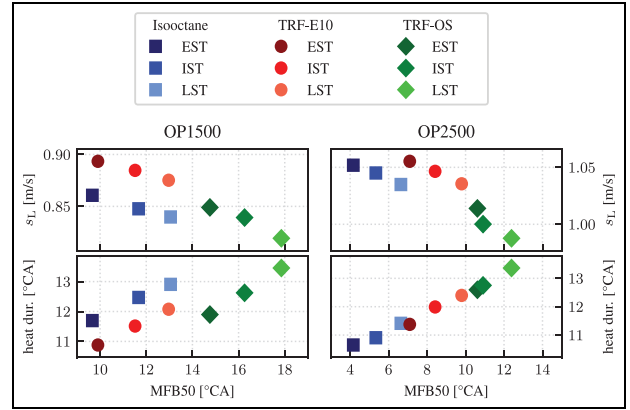
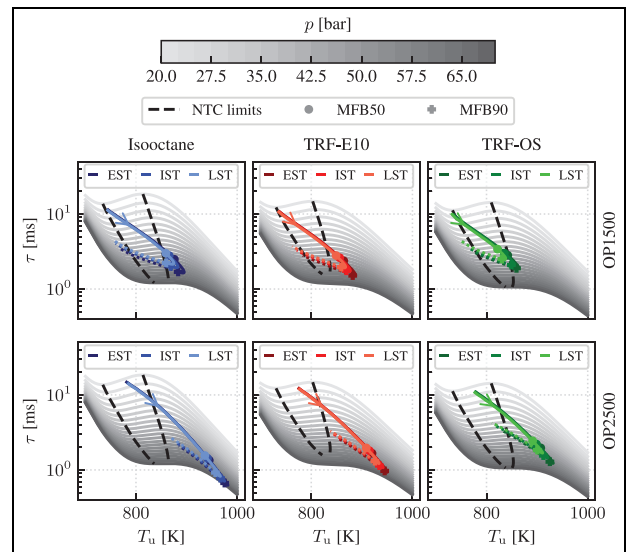
To retrieve the laminar burning velocities and auto-ignition delay times for the thermodynamic conditions of the operating points investigated, 1-D laminar freely propagating flame and 0-D homogeneous reactor calculations are performed using a detailed mechanism.<sup>25</sup> As thermodynamic conditions, the average pressure of the measured 1000 cycles per operating point is used along with the unburned temperature calculated with the engine simulation tool GT-Power.

In further analysis of the experimental data, the fuel influence on the heat duration is investigated. Subsequently, the auto-ignition delay times are analyzed under the engine operating conditions. The section closes with a discussion of the NTC influence on a potential auto-ignition event.

### Fuel influence on heat duration

The flame propagation speed inside an engine is influenced by the spark ignition in the initial phase of combustion, while heat transfer at the cylinder wall is important in the final phase. For the in-between interval, the flame propagates freely. Assuming similar turbulent intensities for all operating conditions, the laminar burning velocity  $s_L$  at MFB50 serves as an estimate for the flame propagation speed.<sup>37</sup> In Figure 6,  $s_L$  is depicted, together with the experimental heat duration (cf. Figures 4 and 5) to investigate the fuel influence on the mass burn rate. This analysis is performed for all OPs (see Table 4), where the calculations of  $s_L$  are based on the pressures and unburned temperatures at the respective MFB50 (cf. Figure 7 (circles)).

The different knock limits of the fuels lead to different thermodynamic conditions at MFB50. For the individual fuels, an advance of the spark timing correlates with higher pressures and peak temperatures at MFB50

**Figure 6.** Analysis of laminar burning velocity  $s_L$  and heat duration for OPI500 and OP2500.**Figure 7.** Trajectories of thermodynamic conditions during combustion for isooctane (left), TRF-E10 (center), and TRF-OS (right). OPI500 is shown in the top row, OP2500 in the bottom row. The earliest ignition timing in each case is shown in a darker color, the latest in a lighter color.

(cf. Figure 7 (circles)) leading to higher laminar burning velocities.

For OPI500, the TRF-E10 shows the highest  $s_L$ . This correlates well with the lowest heat duration, hence the cycle with the highest mass burn rate observed in the experiments. Isooctane shows slightly higher values of  $s_L$  than the TRF-OS, which matches with the lower heat durations. However, for the TRF-OS, a stronger decrease in  $s_L$  with later MFB50 is observed. This trend agrees with the steeper increase of the heat duration.

For OP2500, similar trends can be observed. The lowest  $s_L$  of the TRF-OS agrees well with the longest heat duration. Isooctane shows a higher sensitivity to the engine speed than TRF-E10. As a result, the laminar burning velocities of these are similar at OP2500. However, in the case of isooctane, the heat duration is affected somewhat more by the change in engine speed than the laminar burning velocity.

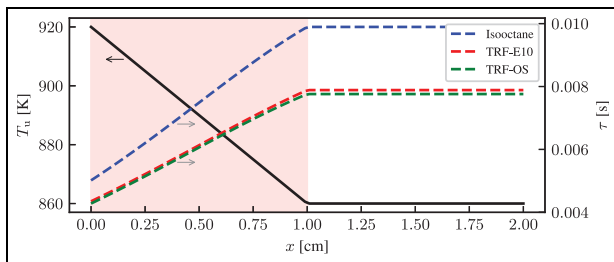


**Figure 8.** Exemplary hot spot at  $p=40$  bar defined by a linear temperature gradient within the interval highlighted in light red. Corresponding auto-ignition delay times of the three surrogate fuels shown as dashed lines. Temperatures are outside the NTC regime for all three surrogate fuels.

In summary, the discussed correlations between laminar burning velocity and heat duration show the fuel influence on the mass burn rate.

### Auto-ignition delay times under engine operating conditions

The fuel influence on auto-ignition delay times under engine operating conditions is investigated for the unburned temperatures and pressures during the combustion process from MFB1 to MFB99. By plotting these as trajectories together with the general sensitivity of the auto-ignition delay times  $\tau$  to unburned temperature  $T_u$  and pressure  $p$  (cf. Figure 1), the potential relevance of the NTC regime is assessed. The analysis for all operation points as listed in Table 4 is depicted in Figure 7.

Isooctane is depicted in the left column, TRF-E10 in the middle column and TRF-OS in the right column. The top row shows results for OP1500, the bottom row for OP2500. The darkest color corresponds to the earliest spark timing, the lightest color to the latest spark timing. The center of the combustion process (MFB50) and MFB90 are marked for every trajectory. The onset of knock is located in the vicinity of the peak pressure in the experiments. For the OPs under investigation, this corresponds to approximately MFB85. Beyond MFB90, no knock initiation was detected in the experiments. Therefore, this interval is not discussed in the following.

As expected, the respective higher pressures and unburned temperatures resulting from earlier spark timings lead to lower auto-ignition delay times during combustion. The relative difference between the fuels correlates with the respective combustion peak pressure.

At OP1500, TRF-E10 shows the highest peak pressure and thus the lowest auto-ignition delay times, TRF-OS has the highest auto-ignition delay times, and isooctane is between the other fuels. At OP2500, the generally earlier spark timing results in more critical thermodynamic conditions. The differences in auto-ignition delay times are larger due to the larger

differences in peak pressure. Now, isooctane shows the lowest auto-ignition delay times, followed by TRF-E10 and TRF-OS.

The order of the auto-ignition delay times does not reflect the order of knock resistance observed in the experiments. While TRF-OS has the lowest knock resistance, it shows the highest auto-ignition delay times for the investigated operating points. Hence, no direct correlation of a lower knock resistance due to lower auto-ignition delay times can be drawn here. However, it is obvious that the thermodynamic conditions of all operating points during combustion are at least partially within the NTC regime. At OP1500, the trajectory of the latest spark timing (LST) of TRF-OS stays within the NTC regime until shortly before the end of combustion. For all other operating points, the tip of the trajectory between MFB50 and MFB90 is just outside the NTC regime. At OP2500, as a consequence of the higher  $T_u$  and  $p$ , a relevant part of the trajectories is beyond the upper NTC limit. However, the initial combustion phase is within the NTC regime for all fuels. Therefore, it is further analyzed how the NTC behavior can affect the auto-ignition process and potentially explain differences in the knock limit.

### NTC influence on auto-ignition

First, the influence of fuel chemistry on the auto-ignition process is discussed based on a 1-D hot spot configuration as commonly used in numerical auto-ignition studies.<sup>8,24</sup> As values for the size of the hot spot and the magnitude of the temperature gradient are not known for the specific conditions, an exemplary hot spot is shown in Figure 8 to provide a more general assessment.

Within the hot spot radius ( $x \leq 1$  cm), the temperature decreases linearly from the peak temperature  $T_u = 920$  K to the uniform temperature of the surrounding  $T_u = 860$  K, as shown by the solid black line. At a pressure of 40 bar, these temperatures are outside the NTC regime for the surrogates investigated. The spatial gradient of the auto-ignition delay time  $\partial\tau/\partial x$  results from the product of the spatial temperature gradient  $\partial T_u/\partial x$  and the gradient of the auto-ignition delay times with respect to the unburned temperature  $\partial\tau/\partial T_u$  (cf. Figure 1):

$$\frac{\partial\tau}{\partial x} = \frac{\partial T_u}{\partial x} \frac{\partial\tau}{\partial T_u} \quad (1)$$

Thus, the spatial gradient of the auto-ignition delay time is fuel-dependent for a given temperature gradient, as shown by the dashed lines in Figure 8. The lowest auto-ignition delay times are observed where the temperature is highest. Therefore, the left boundary of the hot spot auto-ignites first.

The findings of Dai et al.<sup>24</sup> have shown that for fuels with NTC behavior, cool spots may initiate auto-ignition in addition to hot spots. Figure 9 shows an



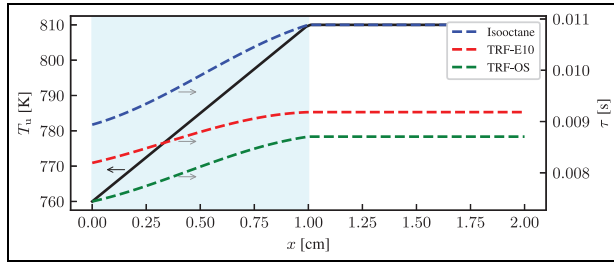


**Figure 9.** Exemplary cool spot at  $p=25$  bar defined by a linear temperature gradient within the interval highlighted in light blue. Corresponding auto-ignition delay times of the three surrogate fuels shown as dashed lines. Temperatures are inside the NTC regime for all three surrogate fuels.

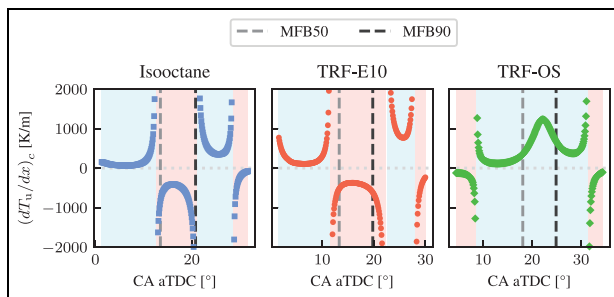


**Figure 10.** Critical temperature gradient over crank angle for the three surrogate fuels at OP1500 and the latest spark timing each (cf. Table 4). Intervals with a positive value for the critical temperature gradient are highlighted in light blue, for a negative value in light red. MFB50 and MFB90 are marked with dashed lines for orientation.

exemplary configuration for such a cool spot. The temperature increases linearly from 760 K at the left boundary, to 820 K at the edge of the cool spot. At a pressure of 25 bar, the three surrogates show NTC behavior, where the auto-ignition delay times increase with increasing temperature. Thus, the reversed sign of  $\partial\tau/\partial T_u$  leads to the same sign for the spatial gradient of auto-ignition delay times as for the hot spot, discussed previously. Consequently, the left boundary of the cool spot auto-ignites first, again.

### Critical temperature gradient analysis

The propagation velocity  $u_a$  of an auto-igniting mixture is crucial for the evolution of the propagation mode after auto-ignition. Neglecting mass diffusion and heat conduction, it is directly proportional to the spatial gradient of the auto-ignition delay time<sup>38</sup>:

$$u_a = \left( \frac{\partial\tau}{\partial x} \right)^{-1}. \quad (2)$$

A coupling between the auto-ignition front and the generated pressure wave can occur when the reaction front propagates approximately at the speed of sound

a. With this and Equation (1), a critical temperature gradient can be defined as:

$$\left( \frac{dT_u}{dx} \right)_c = a^{-1} \left( \frac{d\tau}{dT_u} \right)^{-1}. \quad (3)$$

A positive sign of the critical temperature gradient indicates that a cool spot is required to initiate an auto-ignition front, while a negative sign signifies that a hot spot is needed. Based on 1-D simulations, Dai et al.<sup>24</sup> showed that the subsequent propagation front after a cool spot auto-ignition can evolve into the same modes as those known from hot spot auto-ignition, and concluded that cool spots may cause knocking combustion in engines operating within the NTC regime.

In engine operation with homogeneous mixtures, temperature gradients are the main influencing factor for the auto-ignition delay. It is assumed that temperature stratification is mainly influenced by the heat transfer in the cylinder. However, even with the same temperature stratification, fuel differences in  $\partial\tau/\partial T_u$  lead to different critical temperature gradients. Hence, knock may develop at different thermodynamic conditions. To further investigate this hypothesis, the critical temperature gradient is calculated over the duration of the combustion process based on the thermodynamic conditions retrieved for the characterization of the operating points (cf. Figure 7).

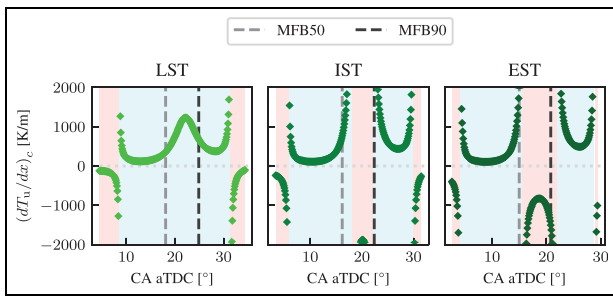
Figure 10 shows the critical temperature gradient for all fuels and OP1500 at the respective latest spark timing (LST). MFB50 and MFB90 are marked as vertical lines.

For isooctane and TRF-E10, the development of the critical temperature gradient is similar. At the start of combustion, the gradient has a positive sign, indicating that a cool spot would initiate auto-ignition, which is highlighted by a light blue background. Just before MFB50, the thermodynamic conditions leave the NTC region (cf. Figure 7), leading to a singularity. Until shortly after MFB90, the critical temperature gradient is negative. A hot spot would initiate auto-ignition for these thermodynamic conditions, which is illustrated by a light red background.

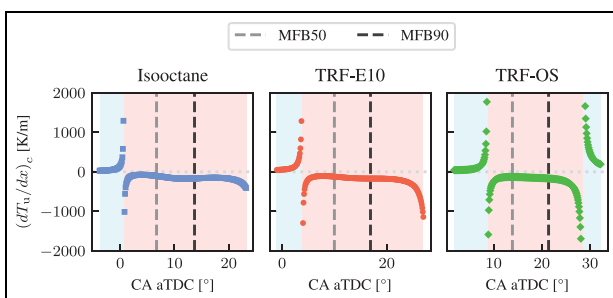
The critical temperature gradient of TRF-OS differs significantly. As shown in Figure 7, the thermodynamic conditions remain within the NTC regime during combustion. As a result, the critical temperature gradient is positive throughout the phase of interest. With this, the thermodynamic conditions may lead to auto-ignition initiated by a cool spot. This suggests, that although the fuels exhibit a comparable knock intensity, this may result from a different initiation process for TRF-OS.

Figure 11 shows the same analysis as before, but for the three different spark timings of TRF-OS at OP1500.

At advanced spark timing (cf. IST and EST), the combustion trajectory leaves the NTC regime. As for the other fuels, the critical temperature gradient between MFB50 and MFB90 is negative. However, the



**Figure 11.** Critical temperature gradient over crank angle for TRF-OS at OPI500 and all three spark timings. Intervals with a positive value for the critical temperature gradient are highlighted in light blue, for a negative value in light red. MFB50 and MFB90 are marked with dashed lines for orientation.



**Figure 12.** Critical temperature gradient over crank angle for the three surrogate fuels at OP2500 and the latest spark timing each. Intervals with a positive value for the critical temperature gradient are highlighted in light blue, for a negative value in light red. MFB50 and MFB90 are marked with dashed lines for orientation.

respective interval is smaller than for the other surrogates. This indicates that auto-ignition at a cool spot may occur at a later stage of the combustion process.

At the higher engine speed of OP2500, combustion of all three surrogates occurs mainly at thermodynamic conditions beyond the NTC regime (cf. Figure 7). As a result, the critical temperature gradient is mostly negative for all fuels, as exemplified in Figure 12 for the latest spark timing (LST). Again, isooctane and TRF-E10 show very similar behavior, while TRF-OS differs slightly, showing the first singularity closer toward MFB50.

In summary, the critical temperature gradient analysis shows that auto-ignition may be initiated by different mechanisms due to the NTC behavior of the surrogate fuels. For OP2500, hot spot auto-ignition appears to be predominant due to thermodynamic conditions outside the NTC. For OPI500, especially for TRF-OS, cool spot auto-ignition may occur. This suggests that auto-ignition may start in different areas of the cylinder, which could explain the different knock resistances observed. A detailed evaluation of the significance of auto-ignition initiated by cool spots or hot spots for the conditions studied is not the scope of this work, as information on the local temperature

distribution cannot be deduced with sufficient accuracy from the available experimental data. Future studies should therefore provide more details on the local temperature gradients either by optical measurements or highly resolved 3-D CFD data to enable such analysis. Furthermore, this would allow localization of the operating conditions in the Bradley et al.<sup>8</sup> diagram by means of the reactivity parameter  $\varepsilon$  and the resonance parameter  $\xi$ , taking into account the excitation time of the mixture.

## Conclusions

In this work, a combined experimental and model-based analysis of conventional gasoline fuel RON95E10 and three surrogate fuels was conducted based on a single-cylinder research engine operated under knocking conditions. All three surrogate fuels show a distinct NTC regime for engine-relevant thermodynamic conditions.

The experimental campaign systematically investigated the influence of spark timing and engine speed on the combustion and knocking behavior of the fuels. The main experimental findings can be summarized as:

- The knock resistance of the fuels correlates with their respective research octane number (RON).
- Isooctane shows the highest knock resistance and higher sensitivity to the engine speed variation than RON95E10.
- The Toluene Reference Fuel TRF-E10 shows the best match to RON95E10. It is able to reproduce the influence of spark timing and engine speed on combustion and knocking behavior.
- The TRF-OS is much less knock resistant than RON95E10. With isooctane as the main component, this indicates a strong non-linear dependence between the mixture composition and the knock resistance. The strong relative increase in knock resistance at higher engine speed and the low octane sensitivity (OS) suggest a potential influence of the negative temperature coefficient (NTC) behavior.

The experimental database was used to perform further model-based analyses extending the experimental findings:

- Differences in the heat duration can be correlated with the laminar burning velocity of the surrogate fuels.
- The observed trends in auto-ignition delay times do not reflect the order of knock resistance observed in the experiments.
- During combustion, temperature and pressure of the unburned mixture are mostly within the NTC regime at the lower engine speed and are mostly outside the NTC regime at the higher engine speed.

- Analysis of the critical temperature gradient indicates that the NTC behavior may lead to different mechanisms of auto-ignition initiation. At the lower engine speed, cool spot auto-ignition may occur. At the higher engine speed, auto-ignition is assumed to be initiated by hot spots. These different mechanisms could explain the different knock resistances observed.

Future studies should include either optical measurements or 3-D CFD simulations to further investigate this hypothesis.

### Acknowledgements

The work of Magnus Kircher is supported by the Graduate School CE within the Centre for Computational Engineering at Technische Universität Darmstadt.


### Declaration of conflicting interests


The author(s) declared no potential conflicts of interest with respect to the research, authorship, and/or publication of this article.

### Funding

The author(s) disclosed receipt of the following financial support for the research, authorship, and/or publication of this article: Funded by the Deutsche Forschungsgemeinschaft (DFG, German Research Foundation) – Projektnummer 423158633 and 423687744.

### ORCID iDs

Magnus Kircher  <https://orcid.org/0000-0001-9006-8954>

Christian Hasse  <https://orcid.org/0000-0001-9333-0911>

### References

- Fraser N, Blaxill H, Lumsden G and Bassett M. Challenges for increased efficiency through gasoline engine downsizing. *SAE Int J Engines* 2009; 2(1): 991–1008.
- Wang Z, Liu H and Reitz RD. Knocking combustion in spark-ignition engines. *Prog Energy Combust Sci* 2017; 61: 78–112.
- Dalby WE. *The internal combustion engine*. Glasgow and Bombay: Blackie and Son Limited, 1922. DOI: 10.1038/110122a0.
- Heywood JB. *Internal combustion engine fundamentals*. McGraw-Hill, New York, 1988.
- Miller C. *Relation between spark-ignition engine knock, detonation waves, and autoignition as shown by high-speed photography*. Technical Report 855, NACA, 1946.
- Spicher U, Kröger H and Ganser J. Detection of knocking combustion using simultaneously high-speed Schlieren cinematography and Multi Optical Fiber Technique. *SAE Trans* 1991; 100: 569–588.
- König G, Maly RR, Bradley D, Lau AKC and Sheppard CGW. Role of exothermic centres on knock initiation and knock damage. *SAE Tech Pap Ser* 1990; 99: 840–861.
- Bradley D, Morley C, Gu XJ and Emerson DR. Amplified pressure waves during autoignition: relevance to CAI engines. *SAE Trans* 2002; 111: 2679–2690.
- Gu XJ, Emerson DR and Bradley D. Modes of reaction front propagation from hot spots. *Combust Flame* 2003; 133(1-2): 63–74.
- Robert A, Truffin K, Iafrate N, Jay S, Colin O and Angelberger C. Large-eddy simulation analysis of knock in a direct injection spark ignition engine. *Int J Engine Res* 2019; 20(7): 765–776.
- Fontanesi S, d'Adamo A and Rutland CJ. Large-eddy simulation analysis of spark configuration effect on cycle-to-cycle variability of combustion and knock. *Int J Engine Res* 2015; 16(3): 403–418.
- Sarathy SM, Farooq A and Kalghatgi GT. Recent progress in gasoline surrogate fuels. *Prog Energy Combust Sci* 2018; 65: 67–108.
- Robert A, Richard S, Colin O and Poinot T. LES study of deflagration to detonation mechanisms in a downsized spark ignition engine. *Combust Flame* 2015; 162(7): 2788–2807.
- Robert A, Richard S, Colin O, Martinez L and De Francqueville L. LES prediction and analysis of knocking combustion in a spark ignition engine. *Proc Combust Inst* 2015; 35(3): 2941–2948.
- Kircher M, Meindl E and Hasse C. Numerical and experimental study on knocking combustion in turbocharged direct-injection engines for a wide range of operating conditions. *Int J Engine Res* 2021. DOI: 10.1177/14680874211060188
- Lacour C and Pera C. An experimental database dedicated to the study and modelling of cyclic variability in spark-ignition engines with LES. Technical report, SAE technical paper, 2011. DOI:10.4271/2011-01-1282.
- Mehl M, Pitz WJ, Westbrook CK and Curran HJ. Kinetic modeling of gasoline surrogate components and mixtures under engine conditions. *Proc Combust Inst* 2011; 33(1): 193–200.
- Kim D, Westbrook CK and Violi A. Two-stage ignition behavior and octane sensitivity of toluene reference fuels as gasoline surrogate. *Combust Flame* 2019; 210: 100–113.
- Liu S, Hewson JC, Chen JH and Pitsch H. Effects of strain rate on high-pressure nonpremixed n-heptane auto-ignition in counterflow. *Combust Flame* 2004; 137(3): 320–339.
- Ju Y, Sun W, Burke MP, Gou X and Chen Z. Multi-timescale modeling of ignition and flame regimes of n-heptane-air mixtures near spark assisted homogeneous charge compression ignition conditions. *Proc Combust Inst* 2011; 33(1): 1245–1251.
- Law CK and Zhao P. NTC-affected ignition in nonpremixed counterflow. *Combust Flame* 2012; 159(3): 1044–1054.
- Leppard WR. The chemical origin of fuel octane sensitivity. *SAE Trans* 1990; 99: 862–876.
- Mehl M, Faravelli T, Giavazzi F, et al. Detailed chemistry promotes understanding of octane numbers and gasoline sensitivity. *Energy Fuels* 2006; 20(6): 2391–2398.
- Dai P, Chen Z, Chen S and Ju Y. Numerical experiments on reaction front propagation in n-heptane/air mixture with temperature gradient. *Proc Combust Inst* 2015; 35(3): 3045–3052.
- Cai L, Ramalingam A, Minwegen H, Alexander Heufer K and Pitsch H. Impact of exhaust gas recirculation on ignition delay times of gasoline fuel: an experimental and modeling study. *Proc Combust Inst* 2019; 37(1): 639–647.

26. Amer A, Babiker H, Chang J, et al. Fuel effects on knock in a highly boosted direct injection spark ignition engine. *SAE Tech Pap* 2012; 5(3): 1048–1065.
27. Westbrook CK, Mehl M, Pitz WJ and Sjöberg M. Chemical kinetics of octane sensitivity in a spark-ignition engine. *Combust Flame* 2017; 175: 2–15.
28. Szybist JP and Splitter DA. Pressure and temperature effects on fuels with varying octane sensitivity at high load in SI engines. *Combust Flame* 2017; 177: 49–66.
29. Zschutschke Axel, Messig Danny, Scholtissek Arne and Hasse C. Universal Laminar Flame Solver (ULF), 2017. DOI: <https://doi.org/10.6084/m9.figshare.5119855.v2>.
30. Hoppe F, Thewes M, Baumgarten H and Dohmen J. Water injection for gasoline engines: potentials, challenges, and solutions. *Int J Engine Res* 2016; 17(1): 86–96.
31. Thewes M, Muether M, Pischinger S, et al. Analysis of the impact of 2-methylfuran on mixture formation and combustion in a direct-injection spark-ignition engine. *Energy Fuels* 2011; 25(12): 5549–5561.
32. Burkardt P, Ottenwälder T, König A, et al. Toward co-optimization of renewable fuel blend production and combustion in ultra-high efficiency SI engines. *Int J Engine Res* 2021. DOI: 10.1177/14680874211040995
33. Spindt RS. Air-fuel ratios from exhaust gas analysis. *SAE Tech Pap Ser* 1965; 74: 788–793.
34. Bresenham D, Reisel J and Neusen K. Spindt air-fuel ratio method generalization for oxygenated fuels. *SAE Tech Pap Ser* 1998; 107: 2154–2171.
35. Rassweiler GM and Withrow L. Motion pictures of engine flames correlated with pressure cards. *SAE Tech Pap Ser* 1938; 33: 185–204.
36. Mehl M, Chen JY, Pitz WJ, Sarathy SM and Westbrook CK. An approach for formulating surrogates for gasoline with application toward a reduced surrogate mechanism for CFD engine modeling. *Energy Fuels* 2011; 25(11): 5215–5223.
37. Linse D, Hasse C and Durst B. An experimental and numerical investigation of turbulent flame propagation and flame structure in a turbo-charged direct injection gasoline engine. *Combust Theory Model* 2009; 13(1): 167–188.
38. Zeldovich Y. Regime classification of an exothermic reaction with nonuniform initial conditions. *Combust Flame* 1980; 39(2): 211–214.